Journal of Hazardous Materials 176 (2010) 549–558

Contents lists available at ScienceDirect

Journal of Hazardous Materials

journal homepage: www.elsevier.com/locate/jhazmat

Modeling solid thermal explosion containment on reactor HNIW and HMX

Chun-Ping Lin[a], Chang-Ping Chang[c], Yu-Chuan Chou[b], Yung-Chuan Chu[a], Chi-Min Shu[a,b,*]

[a] Doctoral Program, Graduate School of Engineering Science and Technology, National Yunlin University of Science and Technology (NYUST), 123, University Rd., Sec. 3, Douliou 64002, Yunlin, Taiwan, ROC
[b] Process Safety and Disaster Prevention Laboratory, Department of Safety, Health, and Environmental Engineering, NYUST, 123, University Rd., Sec. 3, Douliou 64002, Yunlin, Taiwan, ROC
[c] Department of Applied Chemistry and Materials Science, Chung Cheng Institute of Technology, National Defense University, 190, Sanyuan 1st St., Dashi, 33509, Taoyuan, Taiwan, ROC

ARTICLE INFO

Article history:
Received 16 April 2009
Received in revised form 10 October 2009
Accepted 10 November 2009
Available online 17 November 2009

Keywords:
2,4,6,8,10,12-Hexanitro-2,4,6,8,10,12-hexaaza-isowurtzitane
(HNIW)
Octahydro-1,3,5,7-tetranitro-1,3,5,7-tetrazocine
(HMX)
Thermal explosion hazard
Differential scanning calorimetry (DSC)
Thermokinetic models

ABSTRACT

2,4,6,8,10,12-Hexanitro-2,4,6,8,10,12-hexaaza-isowurtzitane (HNIW), also known as CL-20 and octahydro-1,3,5,7-tetranitro-1,3,5,7-tetrazocine (HMX), are highly energetic materials which have been popular in national defense industries for years. This study established the models of thermal decomposition and thermal explosion hazard for HNIW and HMX. Differential scanning calorimetry (DSC) data were used for parameters determination of the thermokinetic models, and then these models were employed for simulation of thermal explosion in a 437 L barrel reactor and a 24 kg cubic box package. Experimental results indicating the best storage conditions to avoid any violent runaway reaction of HNIW and HMX were also discovered. This study also developed an efficient procedure regarding creation of thermokinetics and assessment of thermal hazards of HNIW and HMX that could be applied to ensure safe storage conditions.

1. Introduction

It is important to study the thermal explosiveness of a reactive chemical in order to ensure safe storage, transportation, and operation. Because this is an important practical aspect of reactive hazard assessment, we did a thermal analysis of 2,4,6,8,10,12-hexanitro-2,4,6,8,10,12-hexaaza-isowurtzitane (HNIW) and octahydro-1,3,5,7-tetranitro-1,3,5,7-tetrazocine (HMX) by differential scanning calorimetry (DSC) [1], applying thermal safety software (TSS) in various scanning rates (1, 2, 4, and 10 °C min^{-1}) for kinetics evaluation [2–6], and then to simulate thermal explosion of a 437 L HMX's final product of barrel reactor and a 24 kg cubic box package [6–10].

The aim was to study thermal decomposition of HNIW and HMX by DSC, then to create the decomposition kinetic models, and finally to employ these models to assess thermal explosion hazard by simulation in order to predict the best storage conditions that allow avoiding any violent runaway reaction. This approach was to develop a precise and effective procedure on thermal decomposition and explosion properties, such as heat of decomposition (ΔH_d), activation energy (E_a), isothermal time to maximum rate (TMR_{iso}), total energy release (TER), time to conversion limit (TCL), self-accelerating decomposition temperature (SADT), control temperature (CT), emergency temperature (ET), and critical temperature (T_{CR}), etc. [2–10] for reactor containing HNIW and HMX.

In particular, this study allowed estimation of runaway parameters at the earliest stages of the life cycle of a chemical product, thus ensuring elimination or significant reduction of the necessity of explosive experiments. These approaches can be applied for many important tasks, such as conceptual design and optimization of chemical processes, reactor design, assessment of reaction hazards, choice of safe conditions of storage and transportation of a commercial chemical, etc.

2. Experimental and methods

2.1. Differential scanning calorimetry (DSC)

Samples of HNIW and HMX were supplied by the National Defense University of the Republic of China (ROC) in Taiwan. Non-isothermal DSC analysis of the samples was made on a Mettler

* Corresponding author at: Doctoral Program, Graduate School of Engineering Science and Technology, NYUST, 123, University Rd., Sec. 3, Douliou 64002, Yunlin, Taiwan, ROC. Tel.: +886 5 534 2601; fax: +886 5 531 2069.
E-mail address: shucm@yuntech.edu.tw (C.-M. Shu).

0304-3894/$ – see front matter © 2009 Elsevier B.V. All rights reserved.
doi:10.1016/j.jhazmat.2009.11.064

Nomenclature

C_P	specific heat capacity ($J\,g^{-1}\,K^{-1}$)
CT	control temperature (°C)
E_a	activation energy ($kJ\,mol^{-1}$)
E_1	activation energy of the 1st stage ($kJ\,mol^{-1}$)
E_2	activation energy of the 2nd stage ($kJ\,mol^{-1}$)
ET	emergency temperature (°C)
f_i	kinetic functions of the ith stage; $i = 1, 2, 3$
$f(\alpha)$	kinetic functions
k_0	pre-exponential factor ($m^3\,mol^{-1}\,s^{-1}$)
k_i	reaction rate constant ($mol\,L^{-1}\,s^{-1}$); $i = 1, 2$
L	characteristic dimension (m)
n	reaction order or unit outer normal on the boundary
NC	number of components
n_i	reaction order of the ith stage, dimensionless; $i = 1, 2, 3$
Q^∞	specific heat effect of a reaction ($J\,kg^{-1}$)
Q_i	reaction calorific effect ($J\,g^{-1}$)
Q_t	heat production rate ($kJ\,kg^{-1}\,min^{-1}$)
Q_0	heat production ($kJ\,kg^{-1}$)
q	heat flow ($J\,g^{-1}$)
r_i	reaction rate of the ith stage ($g\,s^{-1}$); $i = 1, 2, 3, 4$
S	heat exchange surface (m^2)
SADT	self-accelerating decomposition temperature (°C)
T	absolute temperature (K)
T_0	exothermic onset temperature (°C)
T_c	critical temperature (°C)
TCL	time to conversion limit (day)
T_{CR}	critical temperature (°C)
TER	total energy release ($kJ\,kg^{-1}$)
T_e	ambient temperature (°C)
T_f	exothermic final temperature (°C)
TMR_{iso}	time to maximum rate (min)
T_P	peak temperature (°C)
T_{wall}	temperature on the wall (°C)
t	time (s)
U	heat transfer coefficient ($kJ\,min^{-1}\,m^{-2}\,K^{-1}$)
W	heat power ($W\,g^{-1}$)
z	autocatalytic constant

Greek letters

α	degree of conversion
α_i	degree of conversion of the ith stage; $i = 1, 2, 3, 4$
γ	degree of conversion rate
ρ	density ($kg\,m^{-3}$)
λ	heat conductivity ($W\,m^{-1}\,K^{-1}$)
δ	shape factor
χ	heat transfer coefficient ($W\,m^{-2}\,K^{-1}$)
ΔH_d	heat of decomposition ($kJ\,kg^{-1}$)

TA8000 system instrument; the scanning rates selected for the temperature-programmed ramp were 1, 2, 4, and 10 °C min^{-1}. About 1–1.5 mg of the sample was used for acquiring the experimental data. STAR^e software was used to obtain thermal curves [1]. DSC analysis was implemented on the samples sealed in 40 μL aluminum pans, the test cell was sealed manually by a special tool supplied with Mettler's DSC. The range of temperature rise was from 30 to 300 °C for each experiment.

2.2. Reaction kinetic model simulations

The experimental data were processed and the kinetics evaluated by applying TSS developed by ChemInform Saint-Petersburg (CISP) Ltd. The method for the creation of a kinetic model and the algorithms that are employed are clearly described in [5,6]. In particular, it is shown that numerical optimization methods are required to estimate parameters of kinetic models.

2.3. Thermal explosion simulations

The method is thoroughly described by TSS for a solid thermal explosion model and the algorithms that are used [6–10]. The experimental setup is based upon HMX's final reactor product for the domestic arsenal of the ROC in south of Taiwan. The temperature is kept at ca. 35 °C in summer. The reactor is barrel-shaped, the total volume is ca. 437 L, the radius is 0.4 m, the height is 1.2 m, and the shell thickness is 0.04 m.

Consider a reactor of the simplest barrel shape with the following properties: $C_P = 2000\,J\,kg^{-1}\,m^{-3}$, $\lambda = 0.5\,W\,m^{-1}\,K^{-1}$. There is heat exchange on the boundary top, side, and bottom given by the condition of the third kind (Newton's law), the third kind, and the fist kind, respectively: the environment temperature $T_e = 20$ °C, the heat transfer coefficient $\chi = 10\,W\,m^{-2}\,K^{-1}$. The condition bound of ambient temperature was the following: the seal of reactor is ca. 40 °C under room temperature in summer, the seal of reactor is ca. 60 °C in outdoors exposed to sunlight, the overheating environment temperatures are 120 and 150 °C, the temperature for scene of fire is 250 °C.

In addition, consider from HMX's product reactor, HMX was picked up and packed in paper box (ca. 24 kg) for storage and transportation. The reactor is a cubic box, the total volume is ca. 13.8 L, the length is 0.25 m, the width is 0.25 m, the height is 0.25 m, and the shell thickness is 0.0125 m. There is the heat exchange, the environment temperature, the heat transfer coefficient, and the condition bound of ambient temperature under same condition with barrel reactor.

3. Results and discussion

3.1. Determination of HNIW and HMX's thermokinetic parameters

Formal models can explain complex multi-stage reactions that may consist of several independent, parallel and consecutive stages, as is illustrated by the following pattern [2–6].

The initial conditions are as follows:

$$\frac{d\alpha_1}{dt} = r_1 = k_1(T)f_1 \tag{1}$$

$$\frac{d\alpha_2}{dt} = r_1 - r_2; \qquad r_2 = k_2(T)f_2 \tag{2}$$

$$\frac{d\alpha_3}{dt} = r_2 - r_3; \qquad r_3 = k_3(T)f_3 \tag{3}$$

$$\frac{d\alpha_4}{dt} = r_3 \tag{4}$$

At $t = 0$, $\alpha_i = 0$; $\quad i = 1,\ 2,\ 3,\ 4$

where α_1, α_2, α_3, and α_4 are the degree of conversion of a reaction or stage; r_1, r_2, and r_3 are reaction rates of a reaction or stage; k_1, k_2, and k_3 are the rate constants of a reaction or stage; f_1, f_2, and f_3 are the kinetic functions of a reaction or stage.

Simple single-stage reaction: A → B

$$\frac{d\alpha}{dt} = k_0\, e^{-E_a/RT} f(\alpha) \tag{5}$$

$$f(\alpha) = (1-\alpha)^n \quad n\text{th order} \tag{6}$$

$$f(\alpha) = (1-\alpha)^{n_1}(\alpha^{n_2} + z) \quad \text{autocatalytic} \tag{7}$$

Table 1
Results of experimental data for HNIW and HMX's thermal decomposition via STAR^e software by DSC tests.

	Sample							
	HNIW				HMX			
	1[a]	2[a]	4[a]	10[a]	1[a]	2[a]	4[a]	10[a]
T_0 (°C)	212	209	216	222	242	248	257	267
T_P (°C)	233	235	241	247.43	269	274	285	288
T_f (°C)	246	248	248	256.33	272	277	285	293
$\ln(k_0)/\ln(s^{-1})$	87	61	51	87	21	222	85	78
Reaction order, n	−0.42	−0.13	0.39	−0.13	−0.8	0.85	0.32	0.39
E_a (kJ mol^{-1})	390	278	240	390	128	1030	409	378
ΔH_d (kJ kg^{-1})	3062	2969	2431	1304	2077	2011	1908	1896

[a] Scanning rate (°C min^{-1}).

$$f(\alpha) = (1-\alpha)(-\ln(1-\alpha)^n \quad \text{Avrami–Erofeev} \tag{8}$$

where E_a is the activation energy; k_0 is the pre-exponential factor; n_1 and n_2 are reaction order of specific stages; z is the autocatalytic constant [3–6].

A reaction includes two consecutive stages: A → B → C:

$$\frac{d\alpha}{dt} = k_1 e^{-E_1/RT}(1-\alpha)^{n_1}; \qquad \frac{d\gamma}{dt} = k_2 e^{-E_2/RT}(\alpha-\gamma)^{n_2} \tag{9}$$

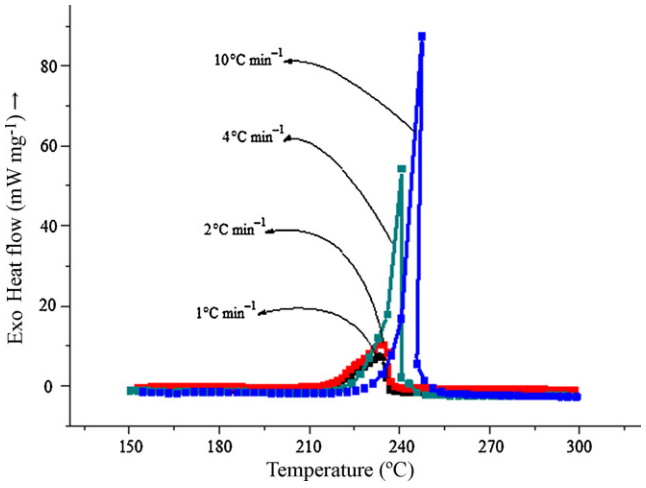

Fig. 1. DSC thermal curves for HNIW decomposition with scanning rates of 1, 2, 4, and 10 °C min^{-1}.

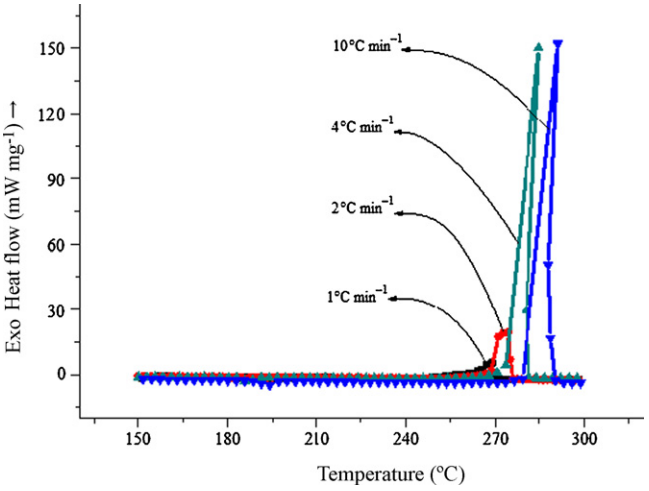

Fig. 2. DSC thermal curves for HMX decomposition with scanning rates of 1, 2, 4, and 10 °C min^{-1}.

where α and γ are degree of conversion of the reactant A and product C, correspondingly; E_1 and E_2 are activation energies of stage one and two.

Two-parallel reactions are a very useful model of full autocatalysis:

$$\frac{d\alpha}{dt} = r_1(\alpha) + r_2(\alpha); \qquad \begin{matrix} r_1(\alpha) = k_1(T)(1-\alpha)^{n_1} \\ r_2(\alpha) = k_2(T)\alpha^{n_2}(1-\alpha)^{n_3} \end{matrix} \tag{10}$$

where r_1 and r_2 are rates of stage one and two; n_3 is reaction order of stage three.

Therefore, we hypothesized that the thermal decomposition for HNIW and HMX belongs to an unknown reaction, such as nth order or autocatalytic reaction. We tried to employ nth order and autocatalytic reaction simulation to compute thermokinetic parameters.

3.2. Different scanning rates (1, 2, 4, and 10 °C min^{-1}) to analyze HNIW and HMX by DSC

Samples of HNIW and HMX were evaluated via DSC with scanning rates of 1, 2, 4, and 10 °C min^{-1}. We acquired thermal decomposition properties, such as onset temperature (T_0), peak temperature (T_P), final temperature (T_f), $\ln(k_0)$, degree of conversion (α) at peak temperature, reaction order (n), activation energy (E_a), and ΔH_d by STAR^e software [1], which are presented in Figs. 1–4 and Table 1. DSC experimental data were processed and then the kinetics was evaluated by applying simulation [2–6].

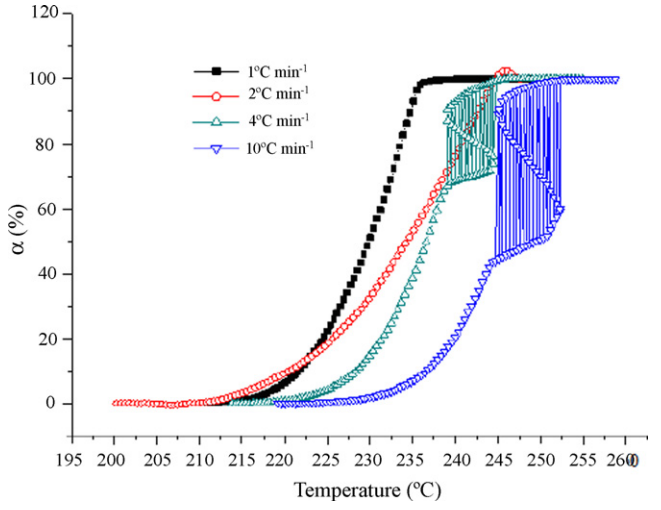

Fig. 3. HNIW's α versus temperature curves with scanning rates of 1, 2, 4, and 10 °C min^{-1} by DSC tests.

Table 2
Results of thermokinetic parameters evaluation for *n*th order and autocatalytic models.

	Sample															
	HNIW								HMX							
	*n*th order				Autocatalytic				*n*th order				Autocatalytic			
	1[a]	2[a]	4[a]	10[a]	1[a]	2[a]	4[a]	10[a]	1[a]	2[a]	4[a]	10[a]	1[a]	2[a]	4[a]	10[a]
$\ln(k_0)/\ln(s^{-1})$	69.2833	60.5754	56.8618	109.1977	25.1163	25.7359	29.5130	23.1852	69.4939	106.3615	38.8528	39.65	24.2032	26.4743	23.5765	24.70
E_a (kJ mol^{-1})	313.8629	278.2512	262.4328	486.9209	127.5549	128.9917	143.5971	111.7084	340.7076	507.0366	199.8086	203.23	135.3177	137.9831	117.8099	123.42
Reaction order, n/*n*th	0.3567	0.3308	1.000E−10	3.003E−08	0.3317	0.5622	1.000E−08	3.259E−07	3.000E−08	1.527E−06	0.0988	0.0243	0.1282	0.8044	1.3058	0.8132
Reaction order (n_1)/auto																
Reaction order, n_2	N/A	N/A	N/A	N/A	0.6033	0.8332	1.0071	0.9801	N/A	N/A	N/A	N/A	0.8739	0.8825	1.5373	1.2059
Autocatalytic constant, z	N/A	N/A	N/A	N/A	3.000E−08	0.0165	0.0347	2.915E−04	N/A	N/A	N/A	N/A	0.0333	8.437E−05	3.733E−04	1.556E−04
ΔH_d (kJ kg^{-1})	3097.8589	3067.6285	2505.7935	1614.7680	3112.5666	2944.1890	3087.0432	1611.8319	2115.5809	2276.0417	2388.7238	2052.28	2151.7300	2258.8658	2503.2316	2112.01

[a] Scanning rate (°C min^{-1}).

Table 3
Results of HNIW for TMR, TER, and TCL at scanning rates of 1, 2, 4, and 10 °C min^{-1} by *n*th order simulation.

Temperature (°C)	Sample: HNIW											
	1[a]			2[a]			4[a]			10[a]		
	TMR (day)	TER (kJ kg^{-1})	TCL (year) (CL = 10%)	TMR (day)	TER (kJ kg^{-1})	TCL (year) (CL = 10%)	TMR (day)	TER (kJ kg^{-1})	TCL (year) (CL = 10%)	TMR (day)	TER (kJ kg^{-1})	TCL (year) (CL = 10%)
20.00	0[b]	3.90E−16	>10	0[b]	1.42E−13	>10	0[b]	2.33E−12	>10	N/A	N/A	N/A
27.27	0[b]	8.82E−15	>10	0[b]	2.24E−12	>10	0[b]	3.13E−11	>10	N/A	N/A	N/A
34.55	0[b]	1.72E−13	>10	0[b]	3.12E−11	>10	0[b]	3.71E−10	>10	N/A	N/A	N/A
41.82	0[b]	2.92E−12	>10	0[b]	3.85E−10	>10	0[b]	3.94E−09	>10	N/A	N/A	N/A
49.09	0[b]	4.37E−11	>10	0[b]	4.23E−09	>10	0[b]	3.75E−08	>10	N/A	N/A	N/A
56.36	0[b]	5.79E−10	>10	0[b]	4.19E−08	>10	>100	3.23E−07	>10	N/A	N/A	N/A
63.64	0[b]	6.88E−09	>10	>100	3.76E−07	>10	>100	2.54E−06	>10	N/A	N/A	N/A
70.91	0[b]	7.35E−08	>10	>100	3.07E−06	>10	>100	1.83E−05	>10	N/A	N/A	N/A
78.18	>100	7.12E−07	>10	>100	2.30E−05	>10	>100	1.21E−04	>10	N/A	N/A	N/A
85.45	>100	6.30E−06	>10	>100	1.59E−04	>10	>100	7.46E−04	>10	N/A	N/A	N/A
92.73	>100	5.10E−05	>10	>100	1.01E−03	>10	>100	4.27E−03	>10	N/A	N/A	N/A
100.00	>100	3.81E−04	>10	>100	6.03E−03	>10	>100	2.28E−02	>10	N/A	N/A	N/A

[a] Scanning rate (°C min^{-1}).
[b] Reaction is extremely slow. In this case TMR for an N-order reaction corresponds to the very beginning of a reaction.

Table 4
Results of HNIW for TMR, TER, and TCL at scanning rates of 1, 2, 4, and 10 °C min^{-1} by autocatalytic simulation.

Temperature (°C)	Sample: HNIW											
	1[a]			2[a]			4[a]			10[a]		
	TMR (day)	TER (kJ kg^{-1})	TCL (year) (CL = 10%)	TMR (day)	TER (kJ kg^{-1})	TCL (year) (CL = 10%)	TMR (day)	TER (kJ kg^{-1})	TCL (year) (CL = 10%)	TMR (day)	TER (kJ kg^{-1})	TCL (year) (CL = 10%)
20.00	>100	1.22E−04	>10	>100	1.06E−04	>10	>100	3.59E−03	>10	>100	5.94E−04	>10
27.27	>100	4.52E−04	>10	>100	4.01E−04	>10	>100	1.24E−02	>10	>100	1.81E−03	>10
34.55	>100	1.59E−03	>10	>100	1.43E−03	>10	>100	4.04E−02	>10	>100	5.25E−03	>10
41.82	>100	5.30E−03	>10	>100	4.83E−03	>10	>100	1.25E−01	>10	>100	1.48E−02	>10
49.09	>100	1.72E−02	>10	>100	1.55E−02	>10	>100	3.70E−01	>10	>100	4.00E−02	>10
56.36	>100	5.58E−02	>10	>100	4.76E−02	>10	>100	1.06E+00	>10	>100	1.07E−01	7.48
63.64	>100	1.87E−01	>10	>100	1.41E−01	>10	>100	3.01E+00	>10	>100	3.08E−01	3.10
70.91	>100	6.84E−01	9.30	>100	4.14E−01	>10	>100	9.34E+00	6.45	>100	1.13E+00	1.33
78.18	>100	2.98E+00	3.63	>100	1.26E+00	7.91	93.44	3.10E+03	2.61	>100	1.06E+01	0.60
85.45	>100	3.22E+01	1.47	>100	4.48E+00	3.11	40.84	3.10E+03	1.10	54.98	1.61E+03	0.27
92.73	45.89	3.06E+03	0.62	97.16	2.99E+03	1.27	18.46	3.10E+03	0.48	26.41	1.61E+03	0.13
100.00	20.41	3.06E+03	0.27	42.07	2.99E+03	0.53	8.61	3.10E+03	0.22	13.05	1.61E+03	0.06

[a] Scanning rate (°C min^{-1}).

Table 5
Results of HMX for TMR, TER, and TCL at scanning rates of 1, 2, 4, and 10 °C min^{-1} by *n*th order simulation.

Temperature (°C)	Sample: HMX											
	1[a]			2[a]			4[a]			10[a]		
	TMR (day)	TER (kJ kg^{-1})	TCL (year) (CL = 10%)	TMR (day)	TER (kJ kg^{-1})	TCL (year) (CL = 10%)	TMR (day)	TER (kJ kg^{-1})	TCL (year) (CL = 10%)	TMR (day)	TER (kJ kg^{-1})	TCL (year) (CL = 10%)
20.00	0[b]	5.42E−21	>10	N/A	N/A	N/A	0[b]	3.85E−09	>10	0[b]	2.00E+01	>10
27.27	0[b]	1.60E−19	>10	N/A	N/A	N/A	0[b]	2.80E−08	>10	0[b]	2.73E+01	>10
34.55	0[b]	4.02E−18	>10	N/A	N/A	N/A	0[b]	1.86E−07	>10	0[b]	3.46E+01	>10
41.82	0[b]	8.69E−17	>10	N/A	N/A	N/A	>100	1.13E−06	>10	0[b]	4.18E+01	>10
49.09	0[b]	1.64E−15	>10	N/A	N/A	N/A	>100	6.30E−06	>10	>100	4.91E+01	>10
56.36	0[b]	2.71E−14	>10	N/A	N/A	N/A	>100	3.27E−05	>10	>100	5.64E+01	>10
63.64	0[b]	3.98E−13	>10	N/A	N/A	N/A	>100	1.58E−04	>10	>100	6.36E+01	>10
70.91	0[b]	5.21E−12	>10	N/A	N/A	N/A	>100	7.13E−04	>10	>100	7.09E+01	>10
78.18	0[b]	6.13E−11	>10	N/A	N/A	N/A	>100	3.03E−03	>10	>100	7.82E+01	>10
85.45	0[b]	6.53E−10	>10	N/A	N/A	N/A	>100	1.21E−02	>10	>100	8.55E+01	>10
92.73	0[b]	6.33E−09	>10	N/A	N/A	N/A	>100	4.60E−02	>10	>100	9.27E+01	>10
100.00	0[b]	5.61E−08	>10	N/A	N/A	N/A	>100	1.67E−01	>10	>100	1.00E+02	>10

[a] Scanning rate (°C min^{-1}).
[b] Reaction is extremely slow. In this case TMR for an N-order reaction corresponds to the very beginning of a reaction.

Table 6
Results of HMX for TMR, TER, and TCL at scanning rates of 1, 2, 4, and 10 °C min^{-1} by autocatalytic simulation.

Temperature (°C)	Sample: HMX											
	1[a]			2[a]			4[a]			10[a]		
	TMR (day)	TER (kJ kg^{-1})	TCL (year) (CL = 10%)	TMR (day)	TER (kJ kg^{-1})	TCL (year) (CL = 10%)	TMR (day)	TER (kJ kg^{-1})	TCL (year) (CL = 10%)	TMR (day)	TER (kJ kg^{-1})	TCL (year) (CL = 10%)
20.00	>100	1.55E−05	>10	>100	1.34E−07	>10	>100	1.43E−04	>10	>100	1.54E−05	>10
27.27	>100	5.96E−05	>10	>100	5.28E−07	>10	>100	4.60E−04	>10	>100	5.25E−05	>10
34.55	>100	2.15E−04	>10	>100	1.95E−06	>10	>100	1.40E−03	>10	>100	1.69E−04	>10
41.82	>100	7.27E−04	>10	>100	6.78E−06	>10	>100	4.06E−03	>10	>100	5.14E−04	>10
49.09	>100	2.34E−03	>10	>100	2.23E−05	>10	>100	1.12E−02	>10	>100	1.49E−03	>10
56.36	>100	7.13E−03	>10	>100	6.95E−05	>10	>100	2.96E−02	>10	>100	4.12E−03	>10
63.64	>100	2.07E−02	>10	>100	2.07E−04	>10	>100	7.50E−02	>10	>100	1.09E−02	>10
70.91	>100	5.78E−02	>10	>100	5.94E−04	>10	>100	1.83E−01	>10	>100	2.79E−02	>10
78.18	>100	1.55E−01	>10	>100	1.65E−03	>10	>100	4.33E−01	>10	>100	6.91E−02	>10
85.45	>100	4.00E−01	>10	>100	4.58E−03	>10	>100	1.00E+00	8.08	>100	1.66E−01	8.60
92.73	>100	1.02E+00	>10	>100	1.24E−02	>10	>100	2.30E+00	3.68	>100	4.01E−01	3.78
100.00	>100	2.58E+00	9.81	>100	3.40E−02	8.46	>100	5.59E+00	1.73	>100	1.04E+00	1.71

[a] Scanning rate (°C min^{-1}).

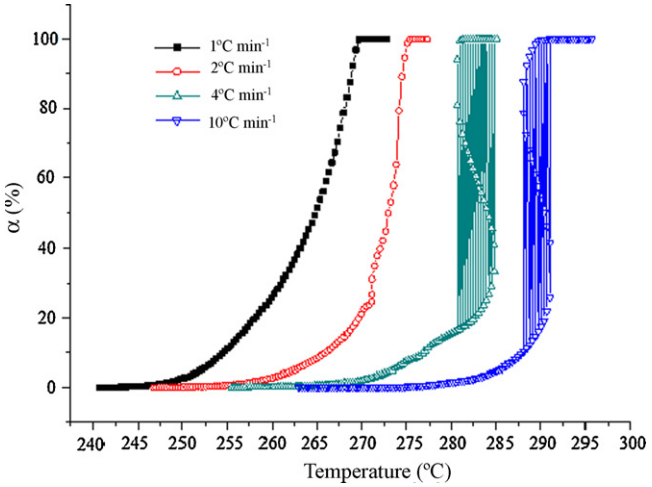

Fig. 4. HMX's α versus temperature curves with scanning rates of 1, 2, 4, and 10 °C min^{-1} by DSC tests.

3.3. Determination of HNIW and HMX's thermokinetic parameters at different scanning rates (1, 2, 4, and 10 °C min^{-1}) by simulation

The HNIW and HMX's thermokinetic parameters were evaluated as listed in Table 2, and then the results of HNIW and HMX's TMR_{iso}, TER, and TCL calculated by applying the models are shown in Tables 3–6. From Table 2, we compared the E_a of thermal decomposition and that in the literature, HNIW and HMX ca. 150–270 kJ mol^{-1} [11–15] and 130–450 kJ mol^{-1} [16–23], respectively. We found that the simulation method could be appropriately used in the thermal decompositions of HNIW and HMX.

Similar to the high performance explosive property of polyazaisowurtzitane, HNIW and HMX have six N–NO_2 groups [11–15] and four N–NO_2 groups [16–23], respectively. Therefore, while the thermal decomposition occurs, products can accumulate in a reacting sample, which promotes acceleration of the reaction. This phenomenon is an important characteristic of an explosive's thermal decomposition.

From Tables 1 and 2 and Figs. 1 and 2, we can see that the greater the scanning rate, the worse the stability and applicability. This is because the greater the scanning rate, the wider and smoother the thermal analysis curve, from neglecting the slight thermal decomposition differences. In addition, from Figs. 3 and 4, for DSC via the

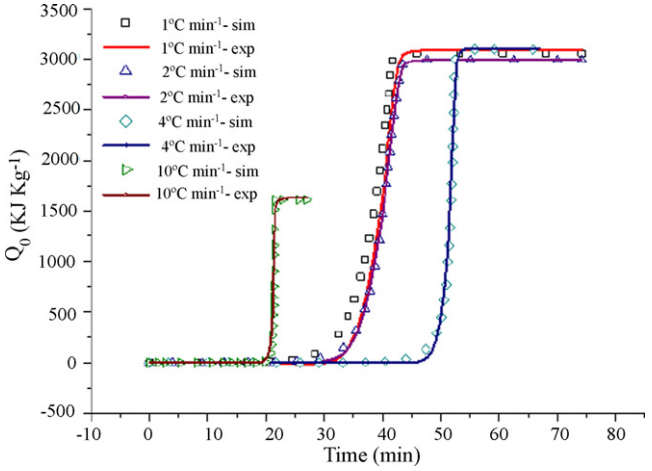

Fig. 5. Comparisons of HNIW's heat production versus time curves of autocatalytic reaction with scanning rates of 1, 2, 4, and 10 °C min^{-1} by experiment and simulation.

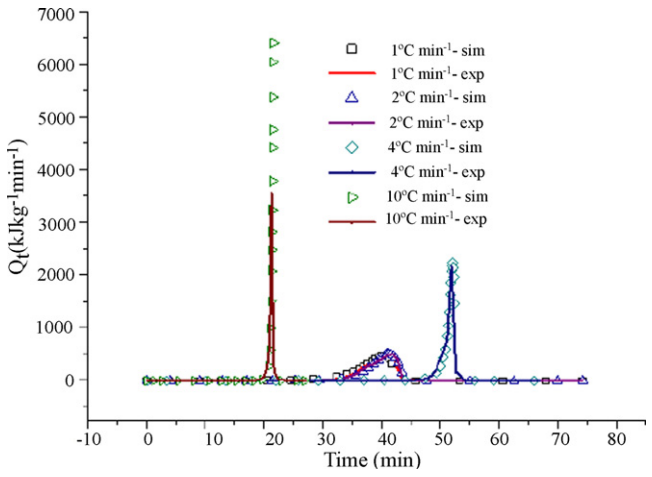

Fig. 6. Comparisons of HNIW's heat production rate versus time curves of autocatalytic reaction with scanning rates of 1, 2, 4, and 10 °C min^{-1} by experiment and simulation.

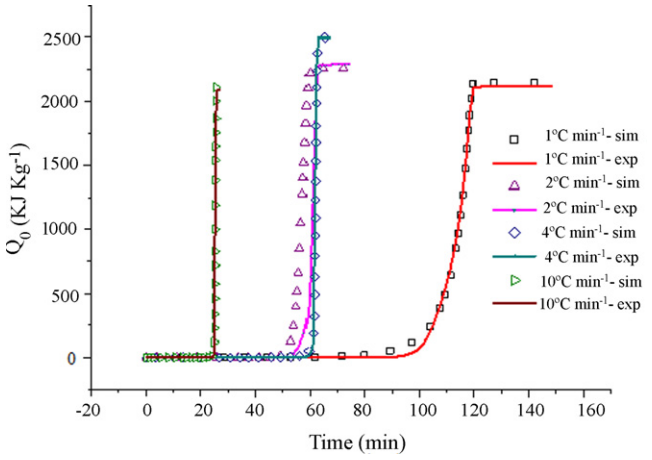

Fig. 7. Comparisons of HMX's heat production versus time curves of autocatalytic reaction with scanning rates of 1, 2, 4, and 10 °C min^{-1} by experiment and simulation.

smaller scanning rate at 1 and 2 °C min^{-1}, the degree of conversion is stable, but a greater scanning rate would be overheating of the sample, so that these data cannot be used for kinetics evaluation.

From Table 2, the results of parameters evaluation for *n*th order reaction and autocatalytic reaction demonstrate that autocatalytic reaction provides much more consistent results for HNIW and HMX. Comparisons of Figs. 5–8 HNIW and HMX's heat production (Q_0) versus time curves and heat production rate (Q_t) versus time of autocatalytic reaction with scanning rates of 1, 2, 4, and 10 °C min^{-1} by experiment and simulation also presented the same result. As far as HNIW and HMX properties of explosives are concerned, too great a scanning rate may induce an auto chain reaction to accelerate the decomposition reaction [23]. Therefore, while analyzing HNIW and HMX thermokinetic parameters of thermal decomposition, we obtained a better condition at lower scanning rates (1 and 2 °C min^{-1}).

In contrast to Tables 3–6, we could observe the results of an *n*th order reaction kinetic simulation and autocatalytic reaction kinetic simulation for HNIW and HMX, in which thermokinetic parameters were providing the results of disorderly and confused by *n*th order reaction simulation. The result is explicit; the *n*th order reaction cannot be appropriately applied on HNIW and HMX's thermokinetic parameter evaluation.

Meanwhile, we also acquired which, HNIW's TMR_{iso} at scanning rate of 1 and 2 °C min^{-1} is ca. less than 85.45 °C, which exceeds the upper limit of 100 days, and HMX's TMR_{iso} at scanning rate of 1 and 2 °C min^{-1} is ca. less than 100 °C, which exceeds the upper limit of 100 days; HNIW's TCL at scanning rate 1 °C min^{-1} is ca. less than 63.64 °C, which exceeds the upper limit of 10 years, scanning rate at 2 °C min^{-1} is ca. less than 70.91 °C, which exceeds the upper limit of 10 years, and HMX's TCL at scanning rate of 1 and 2 °C min^{-1} is ca. less than 92.73 °C, which exceeds the upper limit of 10 years, and then could be applied on the ambient temperature setup condition for storage and transportation.

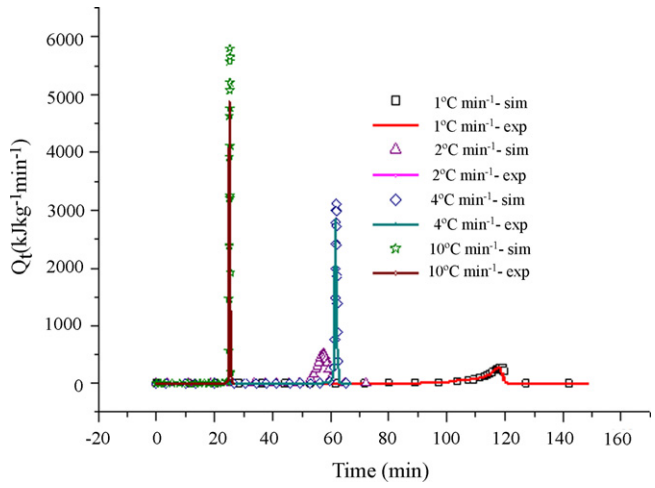

Fig. 8. Comparisons of HMX's heat production rate versus time curves of autocatalytic reaction with scanning rates of 1, 2, 4, and 10 °C min^{-1} by experiment and simulation.

While analyzing HNIW and HMX's thermokinetic parameters by TSS, we obtained a better condition at a scanning rate of 1 and 2 °C min^{-1} applied on the thermal explosion simulation. Meanwhile, we found that the DSC tests and TSS simulation results presented a check of ΔH_d at the scanning rates of 1 and 2 °C min^{-1}.

3.4. Determination of thermal explosion parameters by simulation

To simulate thermal explosions in solids, the critical parameters of thermal explosion are found numerically in the context of complicated chemical kinetics for several types of the reactor geometry, various boundary conditions, and with the possibility to set inert partitions or shells. Analytical and computer-based methods for thermal explosion hazard assessment were compared, and the weakness of the analytical approach and the necessity of using the full numerical investigation are shown [7]. Considering solid thermal explosion simulation, they made the following statement.

The process model is the following:

$$\rho C_P \frac{\partial T}{\partial t} = \mathrm{div}(\lambda \Delta T) + W \quad \text{thermal conductivity equation} \tag{11}$$

$$\frac{\partial \alpha_i}{\partial t} = r_i \quad i = 1, \ldots, \mathrm{NC} \quad \text{kinetic equations (formal models)} \tag{12}$$

$$W = \sum_{(i)} Q_i^{\infty} r_i \quad \text{heat power equation} \tag{13}$$

where T is the temperature; t is the time; ρ is the density; C_P is the specific heat; λ is the heat conductivity; Q_i is the reaction calorific effect; W is the heat power; r_i is the reaction rate; α is the degree of conversion of a component; NC is the number of components; i is the component number.

Table 7
Boundary conditions for barrel reactor and cubic box package.

Reactor shape	Boundary conditions	χ (W m^{-2} K^{-1})	Ambient temperature (°C)					Initial temperature (°C)
Barrel	Top/3rd kind	10	40	60	120	150	250	20
	Side/3rd kind	10	40	60	120	150	250	
	Bottom/1st kind	–	20	20	20	20	20	
Cubic box	Top/3rd kind	10	40	60	120	150	250	20
	Sides/3rd kind	10	40	60	120	150	250	
	Bottom/1st kind	–	20	20	20	20	20	

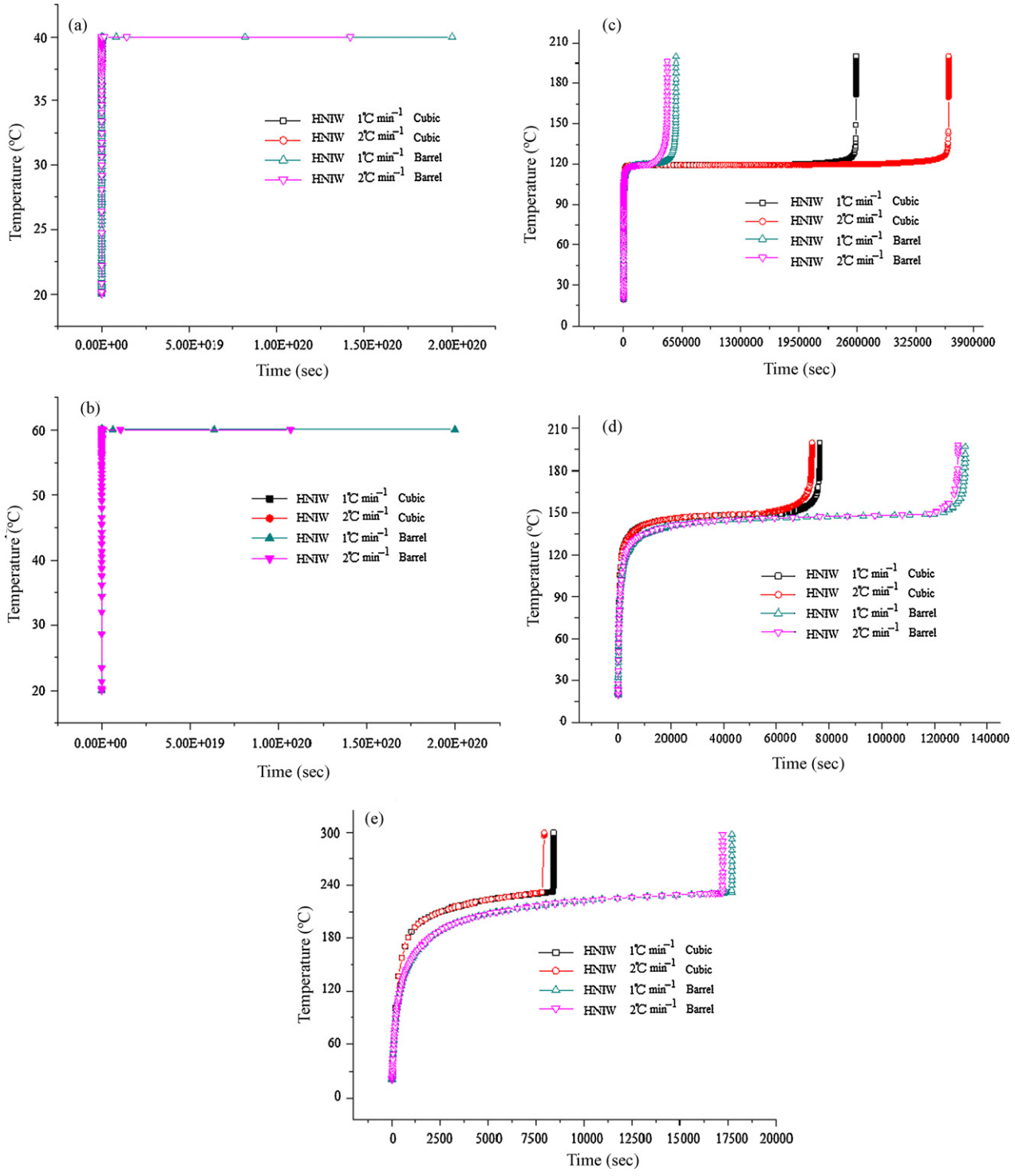

Fig. 9. Thermal explosion simulation by runaway reaction graphs of HNIW with barrel reactor and cubic box at ambient temperature (a) 40 °C, (b) 60 °C, (c) 120 °C, (d) 150 °C, and (e) 250 °C, respectively.

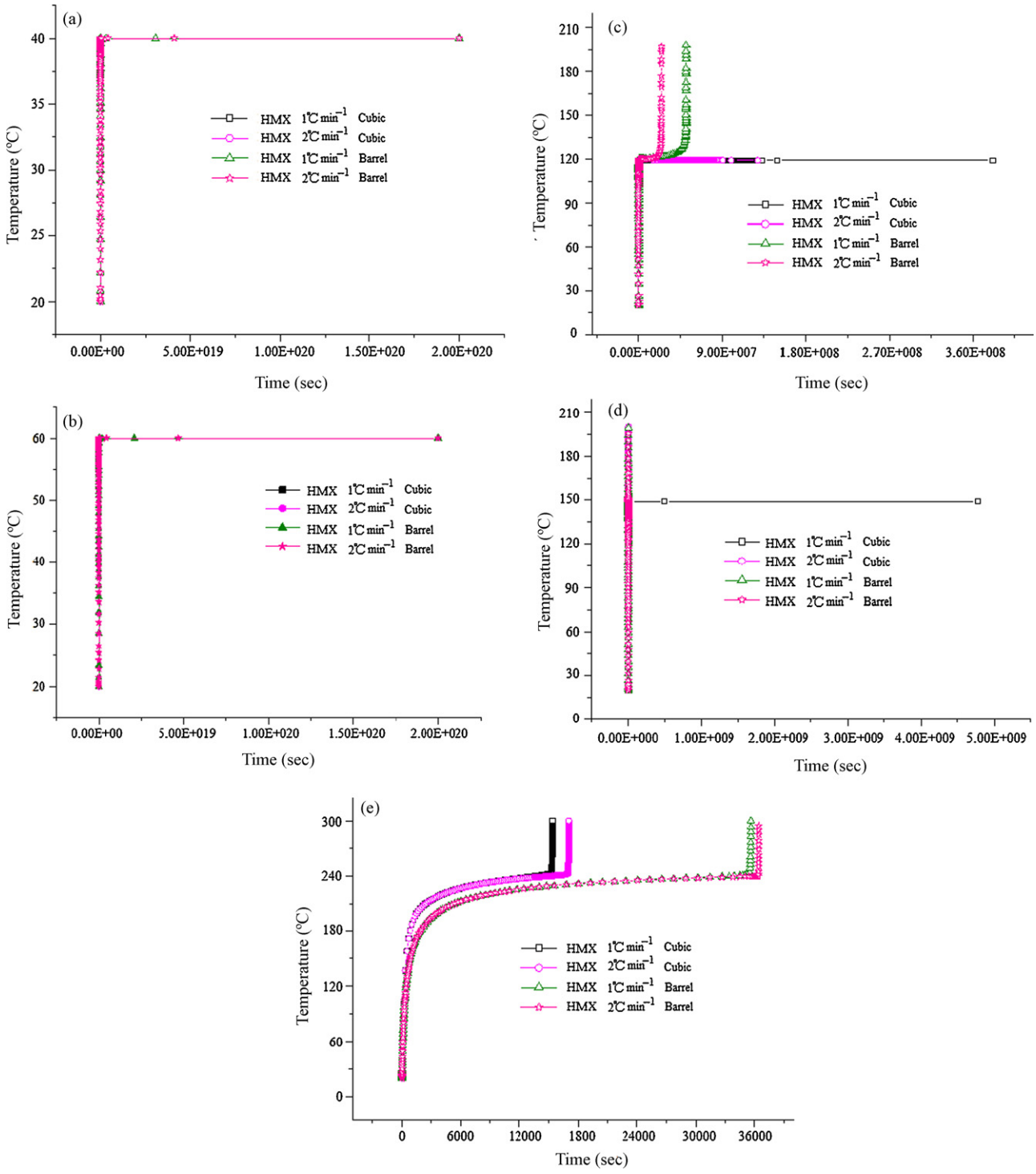

Fig. 10. Thermal explosion simulation by runaway reaction graphs of HMX with barrel reactor and cubic box at ambient temperature (a) 40 °C, (b) 60 °C, (c) 120 °C, (d) 150 °C, and (e) 250 °C, respectively.

Table 8
Results of thermal explosion simulation for HNIW and HMX's SADT, CT, ET, and T_{CR}.

Shape	Sample	DSC scanning rate	SADT (°C)	CT (°C)	ET (°C)	T_{CR} (°C)
Barrel reactor	HNIW	1 °C min^{-1}	110	100	105	87.4
		2 °C min^{-1}	108	98	107	85.3
	HMX	1 °C min^{-1}	140	130	135	115.8
		2 °C min^{-1}	148	138	143	108.8
Cubic box	HNIW	1 °C min^{-1}	118	108	113	108.2
		2 °C min^{-1}	119	109	114	110.1
	HMX	1 °C min^{-1}	155	145	150	145.1
		2 °C min^{-1}	154	144	149	139.1

Initial fields of the temperature and conversions are supposed to be constant through the reactor volume:

$$T|_{t=0} = T_0$$
$$\alpha_i|_{t=0} = \alpha_{i0} \quad (14)$$

Here, the index 0 marks initial values of the temperature and conversion.

The boundary conditions of the first, second, or third kind can be specified:

$$\text{1st kind}: \quad T_{\text{wall}} = T_{\text{e}}(t) \quad \text{temperature} \quad (15)$$

$$\text{2nd kind}: \quad q|_{\text{wall}} = q(t) \quad \text{heat flow} \quad (16)$$

$$\text{3rd kind}: \quad -\lambda \left.\frac{\partial T}{\partial n}\right|_S = \chi(T_{\text{wall}} - T_{\text{e}})$$

Newton's law of heat exchange (17)

Here the indices "wall" and "e" relate to the parameters on the boundary and in environment, respectively; q is the heat flow; n is the unit outer normal on the boundary [6–10].

3.5. Determination of HNIW and HMX's thermal explosion parameters by simulation

The method for estimation of the thermal explosion parameters based on the Frank–Kamenetskii theory is well recognized [9]. Analytical evaluations of the critical conditions are also known for bodies of the simplest form and constant boundary conditions of the first and third kind. For bodies of complex form consisting of elements with various thermophysical properties, it may be rather difficult to obtain analytical evaluations [6–10].

According to the experimental setup we were given, HNIW and HMX ambient temperature is ca. 40 °C in the south of Taiwan, the seal of reactor is ca. 60 °C in summer, the overheating environment temperature is 120 and 150 °C, and the temperature for scene of fire is 250 °C, respectively. Runaway reaction simulation of boundary condition for shape of barrel reactor and cubic box package is listed in Table 7, and then the thermal explosion simulation by runaway reaction graphs with a barrel reactor and a cubic box are displayed in Figs. 9 and 10. Moreover, results of thermal explosion simulation for HNIW and HMX's SADT, CT, ET, and T_{CR} are presented in Table 8. In addition, from Tables 1 and 2, we determined that HMX's thermal decomposition stability was better than HNIW, but its exothermic quantity for thermal decomposition was smaller. According to Figs. 9 and 10 and Table 8, we confirmed again that HMX's thermal decomposition stability was better. Therefore, the aim was to assess thermal explosion hazard in HMX's final product of reactor and commercial packaging conditions. Simulation results indicating the best storage conditions employed to avoid any violent runaway reaction of HNIW and HMX were discovered. Meanwhile, we found that at a low ambient temperature of storage below 40 and 60 °C HNIW and HMX are stable.

We also obtained HNIW and HMX's T_{CR} for thermal decomposition by two types of reactor shape; the energetic materials such as HNIW and HMX by thermal decomposition can be thoroughly simulated to understand explosion phenomenon. Furthermore, this study developed an efficient procedure for determining thermokinetic parameters and thermal hazard of HNIW and HMX, and could be applied to choose the safest storage conditions.

4. Conclusions

The thermal explosion of HNIW and HMX was studied by simulation. TSS simulation was fully exploited to model the kinetic parameters and safety parameters precisely to provide hazard information on how to prevent accidents from occurring during transportation or storage. That is different from the conventional nth order kinetic model, because it can account for a highly energetic material's complex autocatalytic reactions.

We established an accurate analysis model on thermokinetic and thermal explosion parameters of HNIW and HMX for the simulation method. We also discovered adequate scanning rates on acquiring thermal decomposition parameters for an energetic chemical of interest, which is a highly elaborate way to analyze the thermokinetic parameters for energetic materials. Data processing, kinetics evaluation, and estimation of k_0, E_a, n_1, n_2, ΔH_d, TMR_{iso}, TCL, TER, SADT, CT, ET, and T_{CR}, etc., were implemented by simulation.

Acknowledgements

The authors are indebted to Dr. Yao-Hsun Hung and Dr. Tzu-Wan Ho for technical suggestions on experiments and analyses of HNIW and HMX thermal properties. In addition, the authors are grateful to CISP Ltd. in St. Petersburg, Russia and National Defense University of ROC in Taiwan.

References

[1] STARe Software with Solaris Operating System, Operating Instructions, Mettler Toledo, Sweden, 2004.
[2] Y.F. Lin, J.M. Tseng, T.C. Wu, C.M. Shu, Effects of acetone on methyl ethyl ketone peroxide runaway reaction, J. Hazard. Mater. 153 (3) (2008) 1071–1077.
[3] A.A. Kossoy, T. Hofelich, Methodology and software for reactivity rating, Process Saf. Prog. 22 (4) (2003) 235–240.
[4] A.A. Kossoy, A.I. Benin, Y.G. Akhmetshin, An advanced approach to reactivity rating, J. Hazard. Mater. 118 (1–3) (2005) 9–17.
[5] A.A. Kossoy, Y.G. Akhmetshin, Identification of kinetic models for the assessment of reaction hazards, Process Saf. Prog. 26 (3) (2007) 209–220.
[6] Thermal Safety Software (TSS), ChemInform Saint-Petersburg (CISP) Ltd., St. Petersburg, Russia, http://www.cisp.spb.ru.
[7] A.A. Kossoy, I. Sheinman, Evaluating thermal explosion hazard by using kinetics-based simulation approach, Process Saf. Environ. Protect. 82 (B6) (2004) 421–430.
[8] A.A. Kosoy, I. Sheinman, Comparative analysis of the methods for SADT determination, J. Hazard. Mater. 142 (2007) 626–638.
[9] D.A. Frank-Kamenetskii, Diffusion and Heat Exchange in Chemical Kinetics, 2nd ed., Plenum Press, New York, USA, 1969.
[10] P.C. Bowes, Self-heating: Evaluating and Controlling the Hazards, Elsevier, New York, USA, 1984.
[11] V.V. Nedelko, N.V. Chukanov, A.V. Raevskii, B.L. Korsounskii, T.S. Larikova, O.I. Kolesova, Comparative investigation of thermal decomposition of various modifications of hexanitrohexaazaisowurtzitane (CL-20), Propell. Explo. Pyrotech. 25 (2000) 255–259.
[12] M.A. Bohn, Kinetic description of mass loss data for the assessment of stability, compatibility and aging of energetic components and formulations exemplified with ε-CL20, Propell. Explo. Pyrotech. 27 (2002) 125–135.
[13] M. Geetha, U.R. Nair, D.B. Sarwade, G.M. Gore, S.N. Asthana, H. Singh, Studies on CL-20: the most powerful high energy material, J. Therm. Anal. Calorim. 73 (2003) 913–922.
[14] R. Turcotte, M. Vachon, Q.S.M. Kwok, R. Wang, D.E.G. Jones, Thermal study of HNIW (CL-20), Thermochim. Acta 433 (2005) 105–115.
[15] J.S. Lee, K.S. Jaw, Thermal decomposition properties and compatibility of CL-20, NTO with silicone rubber, J. Therm. Anal. Calorim. 85 (2) (2006) 463–467.
[16] S. Zeman, Kinetic compensation effect and thermolysis mechanisms of organic polynitroso and polynitro compounds, Thermochim. Acta 290 (1997) 199–217.
[17] A.S. Tompa, W.F. Bryant Jr., Microcalorimetry and DSC study of the compatibility of energetic materials, Thermochim. Acta 367–368 (2001) 433–441.
[18] S. Vyazovkin, C.A. Wight, Model-free and model-fitting approaches to kinetic analysis of isothermal and nonisothermal data, Thermochim. Acta 340–341 (1999) 53–68.
[19] J.S. Lee, C.K. Hsu, C.L. Chang, A study on the thermal decomposition behaviors of PETN, RDX, HNS and HMX, Thermochim. Acta 392–393 (2002) 173–176.
[20] G. Singh, S.P. Felix, P. Soni, Studies on energetic compounds part 28: thermolysis of HMX and its plastic bonded explosives containing Estane, Thermochim. Acta 399 (2003) 153–165.
[21] R.K. Weese, J.L. Maienschein, C.T. Perrino, Kinetics of the $\beta \rightarrow \delta$ solid–solid phase transition of HMX, octahydro-1,3,5,7-tetranitro-1,3,5,7-tetrazone, Thermochim. Acta 401 (2003) 1–7.
[22] M. Chovancová, S. Zeman, Study of initiation reactivity of some plastic explosives by vacuum stability test and non-isothermal differential thermal analysis, Thermochim. Acta 460 (2007) 67–76.
[23] S.J. Chu, Thermal Analysis of Explosives, Science Press, Beijing, PRC, 1994, p. 12 (in Chinese).